International Journal of Machine Tools & Manufacture 181 (2022) 103932

Contents lists available at ScienceDirect

International Journal of Machine Tools and Manufacture

journal homepage: www.elsevier.com/locate/ijmactool

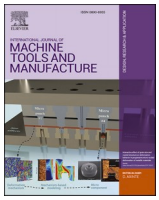

Dual-scale folding in cutting of commercially pure aluminum alloys

Mohammed Naziru Issahaq [a,*], Anirudh Udupa [a], Mojib Saei [b], Debapriya Pinaki Mohanty [a], James B. Mann [c], Narayan K. Sundaram [d], Kevin P. Trumble [a,e], Srinivasan Chandrasekar [a]

[a] Center for Materials Processing and Tribology, Purdue University, West Lafayette, IN, 47907-2023, USA
[b] Department of Mechanical Engineering, Rose-Hulman Institute of Technology, Terre Haute, IN, 47803, USA
[c] M4 Sciences Corporation, Lafayette, IN, 47901, USA
[d] Department of Civil Engineering, Indian Institute of Science, Bangalore, 560012, India
[e] School of Materials Engineering, Purdue University, West Lafayette, IN, 47907-2023, USA

ARTICLE INFO

Keywords:
Folding
Plastic buckling
Stick-slip
Large-strain deformation
Soft metals

ABSTRACT

We examine a, hitherto, little-studied and curious machining chip morphology, with tell-tale signs of folding at two different length scales, that is common in cutting of certain ductile and highly strain-hardening metals like soft aluminum alloys, tantalum and niobium. This chip morphology does not appear in the usual catalogues of common chip types. The mechanics of formation of the "dual-scale folded chip" is studied in model material systems of commercially pure aluminum alloys (AA 1100 and AA 8040), that prominently exhibit this chip morphology. The flow, folding and associated plastic instabilities are investigated using micro/macro structure observations of the chip in a plane-strain cutting framework, with high-speed *in situ* imaging and image analysis of material flow; and force measurements. The smaller-scale folding is shown to develop in the primary deformation zone while the larger-scale folding occurs as the chip traverses the rake face of the tool. The resulting chip is composed of irregularly-spaced large folds, superimposed onto which are the quasi-periodic small folds. The representative wavelengths of the two folds differ on average by an order of magnitude, 0.1 mm vs. 2 mm. The observations reveal a direct coupling between the material flow and chip morphology, and how specific attributes of the dual-scale folded chip arise from the flow mechanism. Plastic buckling is found to play a key role in the folding at both length scales. The small-scale folds are characteristic of a sinuous plastic flow mode, while the large-scale folding is characterized by buckling and stick-slip along the tool rake face, triggered by adhesive pinning of the chip to the tool. Important consequences of the dual-scale folding are very large cutting forces, and force oscillations of large amplitude, despite the alloys being very soft, only ~25 HV. The dual-scale folding is why many of these alloys are classified as "gummy" to machine. Since the dual-scale folded chip is associated with large cutting forces and poor surface quality, there is much to be gained by disrupting this flow type in practical machining applications. Methods for controlling the folding to improve machining performance with the gummy alloys are briefly discussed.

1. Introduction

Chip formation by machining involves large-strain deformation, which spawns a rich variety of flow modes and flow instabilities depending on the mechanical and physical properties of the workpiece alloy [1,2]. The flow mode is important for determining process attributes, such as specific energy and forces, as well as surface quality attributes of the workpiece, e.g., finish, material pull-out and residual plastic strain and microstructure [2–6]. Of course, these process and quality attributes are also critically influenced by other factors such as cutting zone temperature and tool wear (rubbing). It has long been known that the flow mode underlying chip formation is reflected in the chip morphology. For example, unsteady flow modes characterized by shear banding and/or quasi-periodic fracture instabilities give rise to the so-called saw-tooth and segmented chips [3,4,7], while smooth shear-zone/plane deformation with steady laminar flow results in a continuous ribbon chip of near-uniform thickness. This mapping or one-to-one correspondence between the flow mode and chip morphology has been further confirmed by recent *in situ* studies of chip formation using high-speed imaging techniques [4,8,9]. The *in situ*

* Corresponding author.
E-mail address: missahaq@purdue.edu (M.N. Issahaq).

https://doi.org/10.1016/j.ijmachtools.2022.103932
Received 8 May 2022; Received in revised form 6 August 2022; Accepted 9 August 2022
Available online 21 August 2022

observational approach has also revealed new insights. One of these pertains to how an irregular chip morphology, characterized by mushroom-shaped features on the back (free) surface of the chip, and usually observed in cutting of relatively soft and ductile commercially pure metals (e.g., Al, Cu, Fe), arises from an unsteady flow mode called sinuous flow [8]. The sinuous flow involves large-amplitude fold formation in the Primary Deformation Zone (PDZ), triggered by plastic buckling on the workpiece surface [9], and significant redundant straining, both of which result in highly non-uniform, unsteady deformation and large forces/energy. Sinuous flow causes certain highly strain-hardening metals to exhibit poor machinability, despite being soft, thus earning them the "gummy metals" moniker [4,8–10].

The observations and connections between flow and chip morphology suggest that cutting can provide a framework for fundamental study of plastic deformation modes and flow instabilities in metals; and that the chip morphology can serve as a basic signature of the process state. Studies of flow and chip attributes can, of course, be of value also for improving the performance and capability of machining processes, such as by suppression of flow instabilities and improved control of flow modes [3,4,11].

The present study examines a, hitherto, little-studied and curious chip morphology, see Fig. 1, with tell-tale signs of folding on its free surface at two different length scales, that is quite common in cutting of certain ductile and highly strain-hardening metals like tantalum, niobium and soft Al alloys [4,11–14]. This morphology does not appear in the usual lists of chip types [3,15]. The morphology is best described as being composed of (irregularly) recurring fan-shaped large folds (Fig. 1a), onto each fold of which are superimposed numerous sub-folds (Fig. 1b) of much smaller wavelength (small-scale folds). This type of chip, with dual-scale folding, has been observed at both low and high speeds when cutting the afore-mentioned alloys. Clearly, the morphology must arise from a unique underlying flow mechanism(s) and specific flow instabilities.

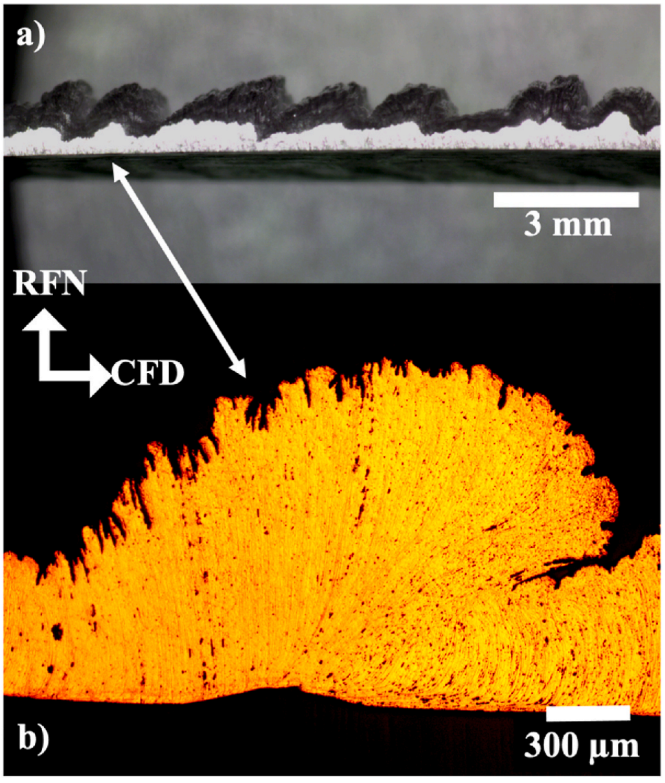

Fig. 1. Dual-scale folding in cutting of soft aluminum Al 1100 alloy. a) Large folds in thickness view of the chip, b) enlarged view of a single large fold with smaller-scale (sub) folds. CFD is chip flow direction and RFN is rake face normal direction. Undeformed chip thickness (t_o) = 125 µm, speed (V_o) = 1 m/s and rake angle (α) = 5°.

We hypothesize, based on fold-morphology observations, that the folding at the two length-scales is controlled by similar pinning mechanisms, i.e., pinning of material flow and occasional plastic buckling. The pinning mode in itself may be quite different for each of the fold length-scales. To examine and validate this hypothesis, we study cutting of commercially pure aluminum alloys (AA 1100 and AA 8040), a model material system, that prominently exhibits this dual-scale folding characteristic. The flow and associated plastic instabilities are investigated using high-speed *in situ* imaging and image analysis; and micro/macro structure observations of the chip and workpiece, and force measurements. The observations reveal a) how specific attributes of the dual-scale folded chip arise from pinning of the material flow - for the small-scale folds, this pinning is found to occur quasi-periodically just ahead of the PDZ, while for the large-scale folds the pinning happens irregularly along the tool rake face; and b) a direct coupling between the flow and chip morphology, as with other chip-types The observations confirm the hypothesis for the dual-scale folding, as arising from flow-pinning followed by plastic buckling. Since the dual-scale folded chip morphology is associated with large cutting forces and poor surface quality, there is much to be gained by disrupting this flow mechanism. Implications of the results for both component machining, and materials manufacturing (e.g., strip and flat wire production) by chip formation, are briefly discussed, along with methods for controlling the dual-scale folding.

2. Experimental details

The mechanics of dual-scale folding and underlying plastic flow are explored through cutting of soft aluminum alloys under plane-strain conditions. The nucleation and evolution of the two types of folds are examined using *in situ* imaging, and *ex situ* observations of chip macro-/micro-structure and force analysis. The deformation conditions are specifically selected to study the folding hypothesis and parametric effects on the folding.

2.1. Workpiece materials

The model material systems are AA 1100 and AA 8040, in the annealed and as-cast conditions, respectively, selected for their propensity to exhibit the dual-scale folding consistently across a range of speeds from low to high (3 mm/s to 6 m/s). The 1100 alloy was acquired as a ¼-in thick plate in the half-hard (H14) condition from McMaster-Carr, Elmhurst, IL, USA. The plate was annealed at 300 °C for 2 h to attain the O-temper condition with hardness 27 ± 2 HV. The 8040 alloy, typically used for production of electrical-conductor wires, was obtained in a commercial as-cast condition, in the form of a wire bar from Prysmian Group (General Cable), Indianapolis, IN, USA. This condition is representative of the softest state (28 ± 1 HV) of the alloy. The two alloys have very similar chemical composition (Table 1) with the main impurity elements (Fe and Si) limited to 1 wt% maximum. The only notable difference is the addition of Zr in the 8040 in amounts that precipitate Al_3Zr particles for purposes of high-temperature strength stability [16]. The similarities of the two alloy systems in terms of composition (Table 1) and strength (hardness <30), while differing in micro/macro structure (wrought vs cast), also made them suitable candidates for comparison under similar deformation conditions.

The fully annealed and as-cast microstructures of the two alloy

Table 1
Chemical composition of workpiece alloys [17].

	Fe	Si	Cu	Mn	Zn	Zr	others	Al
AA1100	1.0		0.05–0.2	0.05	0.1		0.15	rest
AA8040	1.0		0.2	0.05	0.2	0.1–0.3	0.15	rest

workpieces are shown in Fig. 2. The 1100 alloy exhibits an equiaxed grain structure with average grain size of ~50 μm (Fig. 2a). Because Fe and Si are ever-present impurity elements in Al (Table 1) and the solid solubility of Fe in Al is very small (0.05 wt%), phases of Al–Fe or Al–Fe–Si are usually seen in the microstructures of all the 1xxx series alloys except for the super-pure Al [17–19]. Minor impurity elements such as Cu and Mn are not present in sufficient amounts to form their own second phases. For the 8040 alloy, the initial metallography reveals the cast microstructure to contain both columnar and equiaxed grains resulting from directional solidification, as expected (Fig. 2b). During solidification, the columnar grains grow in a preferred crystallographic direction, opposite to the direction in which heat is conducted away. Due to the presence of Zr, precipitates of Al_3Zr can also be seen in the microstructure (Fig. 2b).

2.2. Tool details

The tools were made of M2 high-speed steel. The tool cutting edges were prepared by grinding with edge radius of ~5 μm. This radius is about one-twentieth the undeformed chip thickness, minimizing any edge effects on the chip formation (e.g., plowing). The tool cutting edge width was kept greater than the workpiece width (~6 mm) to ensure plane strain-conditions in the PDZ.

2.3. Deformation conditions and related analysis

Two plane-strain cutting configurations (rotary (high-speed, 1–6 m/s) and linear (low-speed, 3–5 mm/s)) were used in the experiments to study the plastic flow modes and flow instabilities under a range of deformation conditions. The use of the low and high speeds (up to 6 m/s) was to understand deformation rate effects on the folding and flow mode, establish the generality (or lack thereof) of the dual-scale folding phenomenon, and enable process mapping. For the rotary cutting (Fig. 3), disk-shaped workpieces, 6 mm thick x 140 mm diameter, were machined from the annealed plates of the 1100 alloy. Similar disks were cut from 8040 round bar, using a band saw, and then milled to the desired disk diameter and thickness. The 8040 disks remained in the as-cast condition for the machining experiments. Chip formation was effected by feeding a tool radially into the rotating disk workpiece at preset undeformed chip thickness (feed), t_o, as shown in Fig. 3. Various key terms and variables are defined in this figure. A chip of thickness, $t_c > t_o$, resulted; the chip formed by simple shear nominally confined to a narrow deformation region called the Primary Deformation Zone (PDZ) (AB in Fig. 3). The back (free) surface of the chip is shown with corrugations in Fig. 3 to highlight rough surface features that typically result from various flow instabilities. A range of deformation conditions was studied: cutting speeds of 1 m/s to 6 m/s to vary the deformation rate, rake angle (α) of 5° to 45° to vary strain, and t_o set to 100–200 μm. The cutting was done mostly dry (without fluid application), unless otherwise stated. Forces were measured with the cutting tool fixed to a 3-component piezoelectric dynamometer with measuring range up to 10 kN (KISTLER Type 9257B).

Deformation modes under lubricated conditions (lower friction) were examined in low-speed cutting (3 mm/s) using a linear cutting mode. A rectangular plate-shaped workpiece 65 mm (cutting length) x 45 mm × 6 mm (width), cut from the annealed 1100 and cast 8040 alloys, was moved relative to a stationary cutting tool. The cutting fluid was Mobil Vactra Oil No. 1, an oil-based fluid. The fluid was applied close to the tool rake face in a continuous flow mode at a rate of ~5 mL/min. At this low speed, it is relatively easy for the fluid to access the tool-chip interface and lubricate the contact thus enabling the friction effect on flow to be deciphered. The chip formation and underlying material flow were imaged, *in situ*, from a side of the workpiece, through a glass block that was clamped alongside the workpiece length, in order to minimize out-of-plane deformation [9]. A high-speed camera (Photron FASTCAM Mini), coupled to a compact optical microscope (InfiniFlex with high-definition DS 4x lenses of 0.13 NA), was used to make the observations. The working distance of the imaging system from the deformation region of interest was ~20 mm. High-resolution images of the deformation region were obtained at a frame rate of 500 fps. The image sequences were then analyzed using a Digital Image Correlation (DIC) technique to characterize the flow attributes [9,20]. The attributes included velocity, and effective (von Mises) strain and strain rate fields; and flow line mapping in terms of streaklines and pathlines.[1]

Micro- and macro-structures of the workpiece and chip samples were characterized by metallography, and optical and scanning electron microscopy. For this *ex situ* characterization, the samples were mounted in epoxy to avoid heating, ground with various grit sizes of SiC paper, and finally polished with diamond and colloidal silica (0.06 μm). The specimens were etched by immersion in NaOH (10 g in 100 mL H_2O) for 5 min. The microstructure was then observed under an optical microscope. High resolution SEM images of chip surfaces were acquired using a Quanta 650 FEG-SEM. Macrostructure, topography and fold characteristics of the chips were analyzed using optical microscopy (including stereo-imaging) and 3D profilometry (Zygo NewView 9000) to quantify attributes of the dual-scale folding.

3. Results and discussion

A 3D surface profilometer picture of the free (back) surface of an AA 8040 chip, taken at low magnification, is shown in Fig. 4a. Quasi-periodic features of amplitude ~0.7 mm and wavelength ~1 mm are seen to occur along the length of the chip in this region, similar to the surface features in the AA 1100 chip in Fig. 1a. These features arise from a recurring variation in the thickness of the chip. We call each one of these features a large fold, based on similar feature morphologies observed in cutting and sliding [8,14]. The quasi-periodic folded regions were interspersed with other areas where there were very few or no folds. Quantitative details of the thickness variations and dimensional attributes of the large folds are further revealed in the 3D surface profilometer picture of the chip free surface shown in Fig. 4a. Each of the large folds is seen to run across the entire width of the chip. Upon examining these at higher magnification, see Fig. 4a and b, it is evident that each of the large folds is in turn composed of additional surface features of much smaller amplitude (<0.1 mm) and wavelength (<0.2 mm, equivalently higher spatial frequency). These smaller features which ride on the larger folds, and which occur along the entire length of the chip, will henceforth be referred to as small folds, due to the similarity in their morphologies. Thus, the chip free-surface resembles a surface that is formed by repeated folding occurring at two length scales – dual-scale folding – with the small folds superimposed onto the larger fold(s). The use of the term folds to describe these surface features will become clear when we analyze the underlying flow mechanism that leads to the formation of these features.

When observed from the top thickness edge of the chip, the large folds encompass clusters of the small folds (Fig. 4c). The small folds resemble mushroom-like structures when observed in the CFD-RFN plane (Fig. 4b). But they are in fact long interweaving strands of lamellae that run across the width of the chip as seen in the plan view of the chip free surface (Fig. 4c). The large folds cause the chip thickness to be highly non-uniform, consisting of hills and valleys. The thicker regions (peaks) of the large folds are typically more than twice as thick as the thinner regions (valleys). A "shear dimple" is consistently seen directly below each large fold (Fig. 4b), on the underside of the chip that is in contact with the tool rake face. As will be seen in the ensuing, the dimples play an important role in the formation of the large folds.

The chip morphology with dual-scale folding was observed with both

[1] A pathline is the trajectory along which an individual particle (material point) travels, while a streakline is the locus of all particles that have passed through a particular spatial point [9,20].

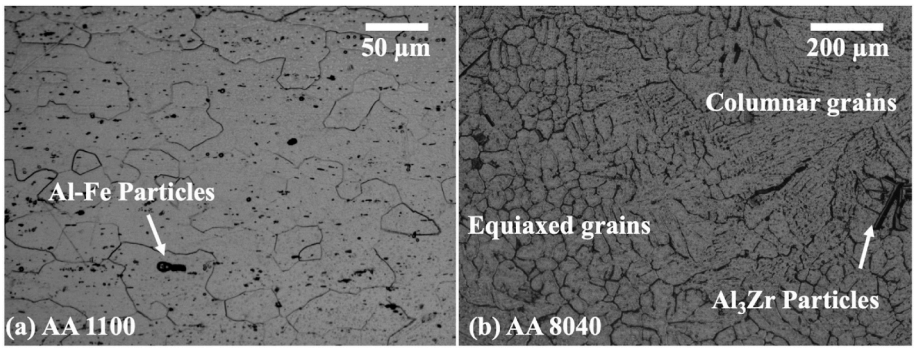

Fig. 2. Optical micrographs showing a) equiaxed microstructure of annealed AA 1100 and b) as-cast microstructure of AA 8040 with both columnar and equiaxed grains, and embedded Al_3Zr particles.

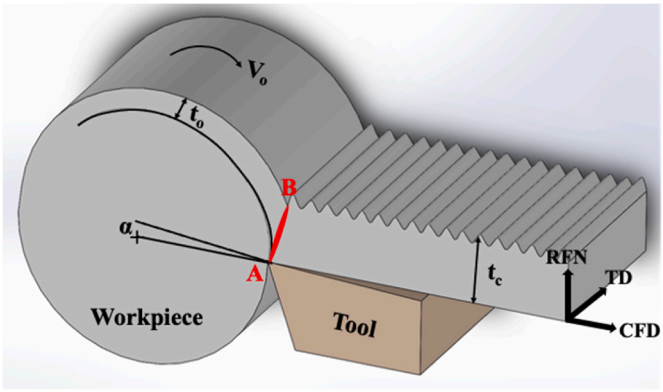

Fig. 3. Schematic of rotary configuration used for plane-strain cutting. The tool is fed radially into the workpiece, as in plunge turning, to produce the chip. Key process variables are defined. Other definitions: nominal primary deformation zone (PDZ) AB; RFN, TD and CFD are the rake face normal, transverse and chip flow directions, respectively.

the Al alloys, and across the spectrum of cutting speeds. This morphology is also common with Ta and Nb alloys [12–14].

3.1. Fold size

Size-related details of the folds were quantified by 3D surface profilometry. The quantification was done in terms of the wavelength (peak-to-peak spacing) and height (amplitude) of the folds. For the wavelength characterization, a Power Spectral Density (PSD) analysis was performed on the 3D chip free-surface (topography) profiles (Fig. 5a) to obtain the spatial frequencies corresponding to the small and large folds. Fig. 5b shows the PSD peaks thus obtained. The average spacing of the small folds, i.e., wavelength, is seen to be ~0.15 mm, and that of the large folds ~2 mm (representative spacing) in the regions where they occur quasi-periodically (Fig. 5b). The large folds have a much larger wavelength than the small folds. It should be noted with the large folds, however, that although in this region of the chip examined (Fig. 5a), they are quasi-periodic with representative wavelength of ~2 mm, this spacing varied significantly (0.8–5 mm range) along the length of the chip. Furthermore, the quasi-periodic regions were typically interspersed with other regions that were nearly devoid of the large folds, see also Supplementary Fig. S2. Hence, the large folds are best described as being stochastic in nature in terms of their overall spacing. This type of variation was noted at every cutting speed condition where the large folds occurred. The stochastic nature of the large folds is to be

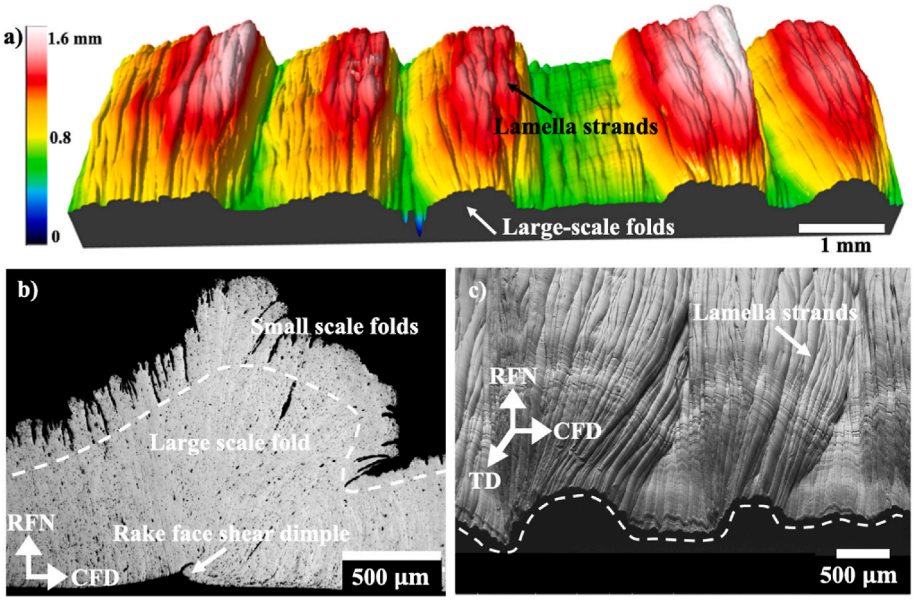

Fig. 4. Macrostructure of chip free (back) surface highlighting key attributes of the dual-scale fold morphology in AA 8040. a) 3D optical profilometer trace of a 10-mm long chip section showing repeating large folds along the chip length and the small folds as lamella strands; b) optical microscope image of a large fold, with smaller (sub) folds resembling mushroom-like structures; and a shear dimple, directly underneath the large fold, on the rake-face side of the chip; and c) plan-view SEM image of the chip free-surface showing the small folds as elongated lamellae along the chip width that cluster together within the large fold. $\alpha = 5°$, $V_o = 6$ m/s and $t_o = 125$ µm.

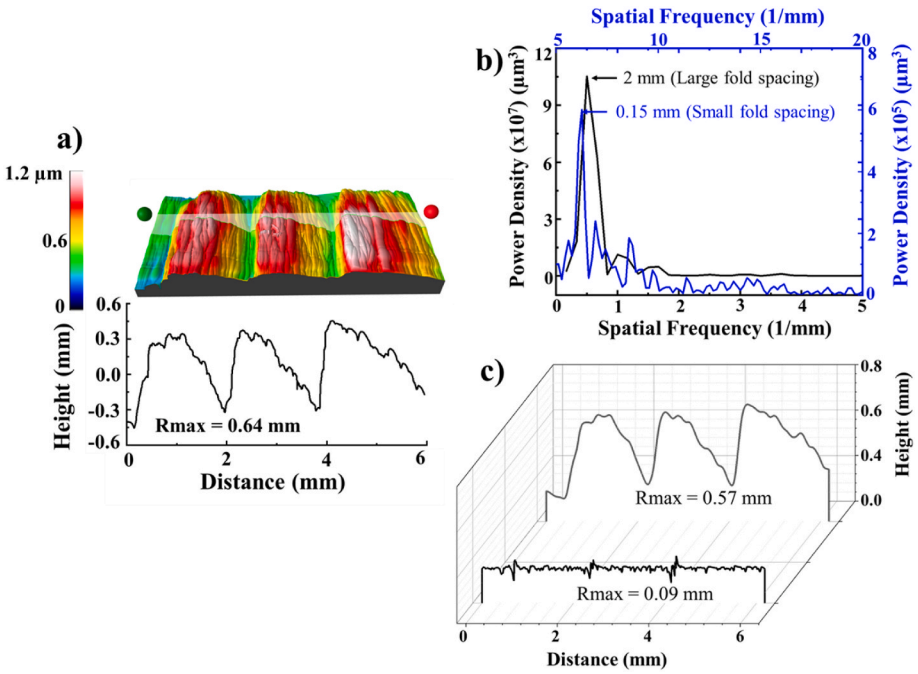

Fig. 5. 3D profile data from chip free surface showing fold attributes. a) Topography of AA 8040 chip surface. b) PSD plots showing spatial frequencies corresponding to the small fold spacing of 0.15 mm and large fold spacing of ~2 mm. c) Filtered FFT surface profiles of the chip free surface in a) using cut-off wavelength (0.15 mm) set equal to the small fold spacing. Peak-to-valley height (Rmax) of small folds = 0.09 mm, and 0.57 mm for the large folds. $\alpha = 5°$, $V_o = 6$ m/s and $t_o = 125$ µm.

contrasted with the largely periodic nature of the small folds.

To determine the height-related (amplitude) information, the small folds were first separated from the large folds in the profiles by a Fast Fourier Transform (FFT) filtering process. The amplitude information was then obtained from the maximum peak-to-valley heights (Rmax) in the filtered profiles. The FFT filtering was done by applying a wavelength cutoff ($\lambda_c = 0.15$ mm) that is approximately equal to the spacing of the small folds, as determined by the PSD analysis. Fig. 5c shows the filtered surface profiles of the high-frequency, small-folds and the information and the residual large fold profile layer. The mean Rmax (amplitudes) values of the small and large folds are 0.09 and 0.57 mm, respectively. The two sets of fold amplitudes differ by a factor of ~6. For this deformation condition, where $t_o = 125$ µm, the large fold corresponds to a thickening of the chip by a factor of ~12 during its formation. This is also indicative of a large strain imposed in the chip. Both the fold amplitude and spacing (wavelength) were usually smaller with the annealed AA 1100 compared to the cast AA 8040 alloy.

It is reasonable to conclude, based on the similarity in the morphology of the two types of folds, that the underlying flow mechanisms for the two folds must have significant common features.

3.2. Fold formation mechanism

Past work using *in situ* imaging, complemented by *ex situ* observations, has shown a one-to-one correspondence between the flow mode and chip morphology in various alloys [3,4]. Hence, we examined the flow pattern and its attributes to determine how the chip morphology features and dual-scale folding arise in the present case.

An initial broad examination of the chip macrostructure under various process conditions showed that the dual-scale folding was the norm at the higher cutting speeds, be it when cutting dry or with a fluid applied. At the lower speeds (e.g., 3 mm/s), however, the large folds did not form when the cutting was done in the presence of the fluid, but did form under conditions of dry (unlubricated) cutting. Also, concomitant with the occurrence of the larger folds was the consistent appearance of a (shear) dimple located mid-way within the larger fold on the chip underside (rake face side), as shown in Fig. 4b. These observations suggested that the origin of the large folds was likely linked to the adhesion/friction condition at the tool-chip interface, with higher adhesion/friction accentuating their formation and development. Earlier *in situ* observations had shown that the small-scale folding in commercially pure metals such as Cu and Fe, and alloys such as stainless steels, arises from a plastic buckling instability on the workpiece surface ahead of the tool, with a sinuous flow mode resulting [4,9]. The nucleation of the buckle, however, was found to be little influenced by the frictional condition at the tool-chip interface. Hence, we hypothesized that the small-scale folds in the present study represent primary folds driven by a plastic flow instability and associated sinuous flow, as in the prior work; and the large-scale folds are secondary folds related to a flow phenomenon that is coupled to the adhesion conditions at the tool-chip contact. The two flow mechanisms then operate in tandem under conditions of higher adhesion/friction to orchestrate the dual-scale folding.

3.2.1. Sinuous flow causes the small folds

To establish whether the smaller-scale surface features on the chip are formed by folding, we carried out *in situ* imaging of the cutting at low speed (3 mm/s) in the presence of a fluid (Mobil Vactra Oil No. 1). At this low speed, the fluid penetrates the tool-chip contact along the rake face providing adequate lubrication. Under such well-lubricated conditions, the large folds did not form, while the small-scale surface features did. This enabled the nucleation and development of the smaller-scale features and underlying flow to be characterized via the *in situ* observations.

Fig. 6 shows four frames from a high-speed image sequence of the low-speed cutting. The sequence of images was analyzed using a digital image correlation (DIC) technique. The images in Fig. 6 show the strain map, along with several overlaid streaklines. It is immediately apparent that the streaklines are highly wavy throughout the chip thickness, indicative of the material folding over repeatedly. The chip is thus comprised of a series of folds stacked on top of one another. The wavy streaklines also mean that the flow is unsteady. It is this type of flow with

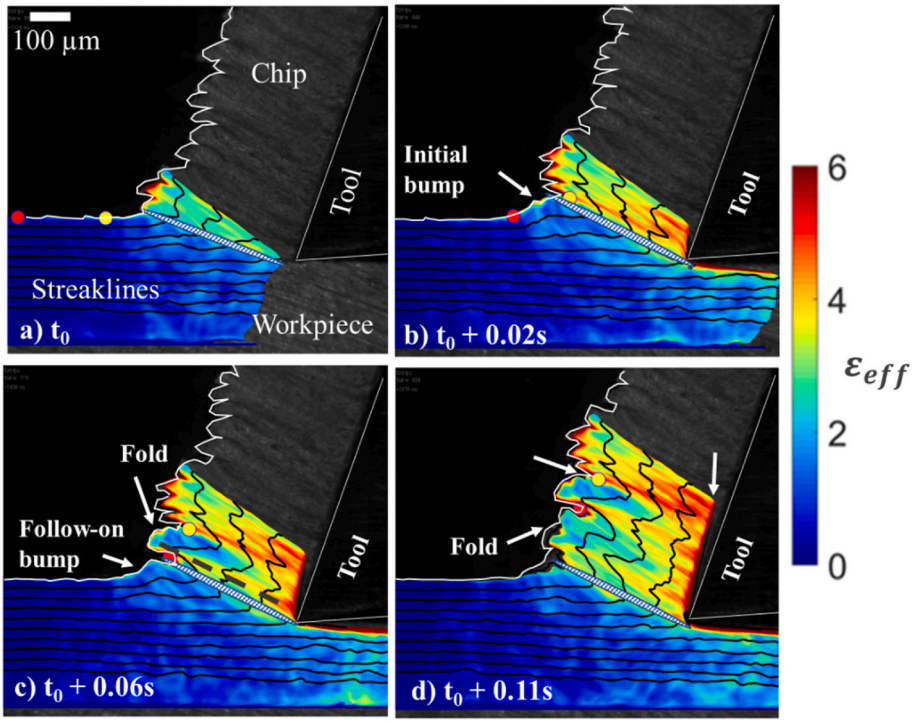

Fig. 6. Select frames from a high-speed image sequence showing development of the small folds in AA 1100 using streaklines. Background color is strain field. $\alpha = 20^{\circ}$, $t_o = 100$ µm, $V_o = 3$ mm/s, fluid – Mobil Vactra Oil No. 1. (For interpretation of the references to color in this figure legend, the reader is referred to the Web version of this article.)

material folding that has been called sinuous flow [8]. The unsteady nature of this sinuous flow is seen in the large variations in von Mises effective strain (between 2 and 6) across the chip thickness. No fracture features are seen in any of the images. The connection between the irregular mushroom-like features on the free surface of the chip, the wavy streaklines, and the material folding explains why we label these surface features as small folds.

The formation of the small folds can be visualized at the mesoscale by following the motion of two points on the workpiece surface – marked with red and yellow circles – ahead of the advancing tool and PDZ

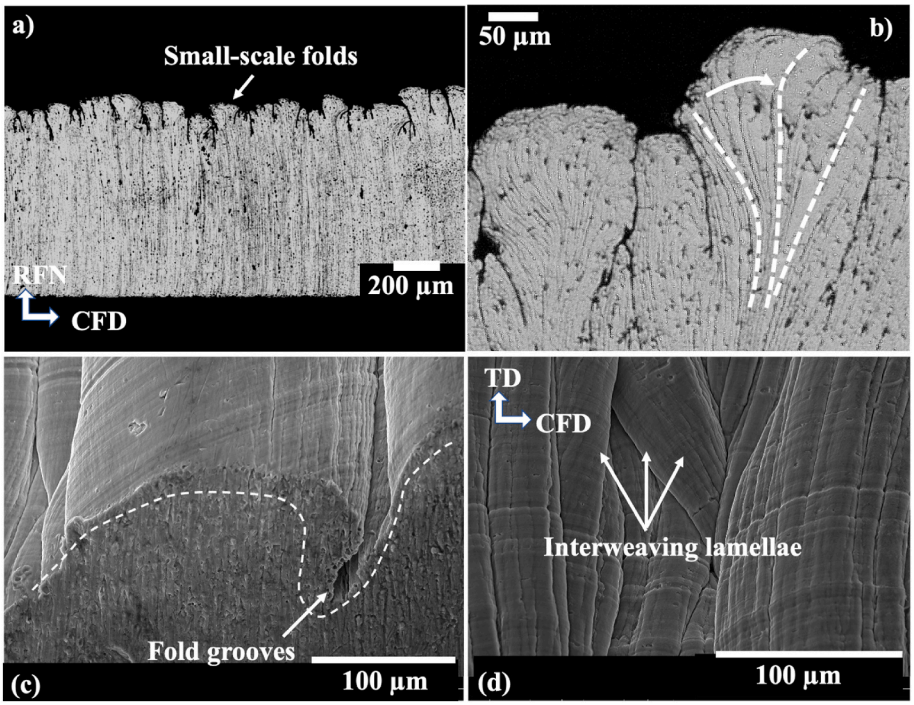

Fig. 7. Micrographs showing small-fold features in AA 8040. a) Overall morphology of the small folds, b) higher magnification image showing the flow line pattern characteristic of the folding mechanism. SEM images showing c) grooves between two consecutive small folds formed by surface plastic deformation, and d) small folds as interweaving strands of lamellae traversing the chip width. Cutting condition: $\alpha = 20^{\circ}$, $t_o = 125$ µm, and $V_o = 3$ mm/s.

(Fig. 6). At time $t = 0$ s, the region between the two points is relatively flat, as it has not entered the deformation zone (**frame a**). In **frame b**, this region has entered the deformation zone and a protuberance (or bump) has formed between the two points. This bump forms by a surface plastic buckling instability that is closely tied to microstructure (grain-level) heterogeneity of flow stress [8]. Simultaneously, all the streaklines immediately underneath this region also begin to form similar buckles indicating that the folding permeates the full thickness of the chip and is not just restricted to the surface. In **frame c**, the bump has grown in size and rotated about the "plane of shear" to become a fold of larger amplitude by the time the material exits the deformation zone. Each surface fold manifests as a mushroom-like surface feature with the amplitude of this feature corresponding to the amplitude of the surface streakline. Also, immediately following and underneath this fully-formed fold, another bump is beginning to form (**frame c**). This bump evolves analogously to eventually form another fold (**frame d**). The process of bump and fold formation repeats quasi-periodically, as is apparent from Fig. 6, indicating that the sinuous flow is not a transient (one-off) phenomenon. The chip thus consists of a series of plastically folded regions that are stacked on top of each other. The small folds are all completely formed by the time the material exits the primary deformation zone. And it is these small folds that appear, in the *ex situ* observations, as mushroom-like structures on the chip free surface in the side view (Fig. 4b).

Fig. 7a is a micrograph of a chip from the lubricated low-speed cutting ($V_0 = 3$ mm/s), that shows the morphology of the small folds. Under this lubricated condition, the large folds do not form. The deformation pattern within each small fold is revealed by the flow line inclinations (Fig. 7b). The flow line inclinations are consistent with the fold development mechanism –a sequence of events involving surface pinning, subsequent buckling in the pinned region, and finally rotation of the fold in the PDZ, as shown by the streakline patterns in Fig. 6. The micrographs of Fig. 7 also clarify the nature of the interfaces between the small folds. It is easy to misconstrue these interfaces (serrations) as cracks and, hence, attribute the formation of these interfaces to recurring fractures. However, Fig. 7c shows that these are actually grooves formed by surface plastic deformation that separate one fold from another. The grooves and interfaces are regions of strain localization, see Fig. 6. In the plan view of the chip free-surface, the small folds appear as lamellar strands that traverse the chip width (Fig. 7d). Again, no evidence for cracking can be seen in this view.

3.2.2. *Large fold formation also occurs by buckling*

To understand the mechanism of how the large folds form, *ex situ* observations were made of the morphology of chips formed at the higher cutting speeds (>1 m/s) under dry cutting conditions. Particular attention was paid to the flow line patterns in the chip. Typically, the deformation in the shear zone (PDZ) is well-reflected in the flow line signatures in the chip bulk.

Optical microscope observations of the large folds (Fig. 8a) at $t_o = 125$ μm and $V_0 = 3$ m/s reveal a flow line pattern that is quite similar to the fan-shaped pattern seen at and near the surface of the small folds (dashed lines in Fig. 7b), but fundamentally different from that of conventional chip formation (laminar flow). In particular, the flow lines in the chip are seen to rotate by ~40° about the shear dimple (depression), see arrow in Fig. 8a, assuming a fan-like morphology centered at the dimple. The extremities of this fan are demarcated by dashed lines in the figure. This suggests that the large fold forms by plastic buckling of the chip material around the dimple, akin to the buckling observed on the workpiece surface ahead of the tool that produces the small folds [9,21]. The claim that plastic buckling is the cause for the large fold formation is unambiguously clear upon reducing the undeformed chip thickness from 125 μm to 50 μm, see Fig. 8b. At this smaller chip thickness, the buckling even causes a section of the chip around the dimple to lift off from the rake face. As a consequence, a crease (self-contact) is seen to form around the dimple by compression of the buckle. Similar plastic buckling and lift-off of the chip, with large-fold (and crease) formation, was also observed at $t_o = 70$ μm. It was only when $t_o > 100$ μm that the buckling occurred without gross lift-off, being confined to the upper part of the chip thickness as in Fig. 8a. This is largely because of an increase in the longitudinal and transverse (structural) stiffness of the chip material at the larger chip thickness.

Additional information about the chip-underside dimple (depression) region in the large folds is obtained from optical profilometry of the free (top) and bottom (underside) surfaces of the chip. Fig. 9a and b shows the topography profiles for the two chip surfaces, respectively. It is clear from these contours that successive dimples on the chip underside are located approximately in the center of successive large folds, i.e., in the middle of the buckle region, consistent with the optical microscope observations. Note that while in the chip side view the dimple appears like a point, it is actually a region of small but finite thickness that runs across the entire width of the chip (Fig. 9b). The maximum vertical height of the dimples is ~80 μm for cutting conditions with $t_o >$ 100 μm. Fig. 9b shows that while the dimpled regions exhibit significant surface coarsening, the regions between the dimples themselves are relatively smooth, indicating intimate contact between the chip and the tool rake face in these areas. A higher magnification SEM micrograph of the dimpled region (Fig. 9c) reveals classical ductile shear fracture characteristics – elongated shear dimples, with the dimples stretched out in the chip flow direction (Note that the use of the word dimple to denote two different features – depression and ductile fracture feature– should not be confusing as the specific reference is clear from the context). The roughened surface is very likely a consequence of shear fracture that occurs at the dimple during the buckling event. The SEM micrograph indicates that the fracture has occurred within the chip material, close to the rake-face contact region with the tool. The reason for referring to this region of the chip underside as a shear-dimple region is now obvious – the combination of a depression, and classical shear-fracture with

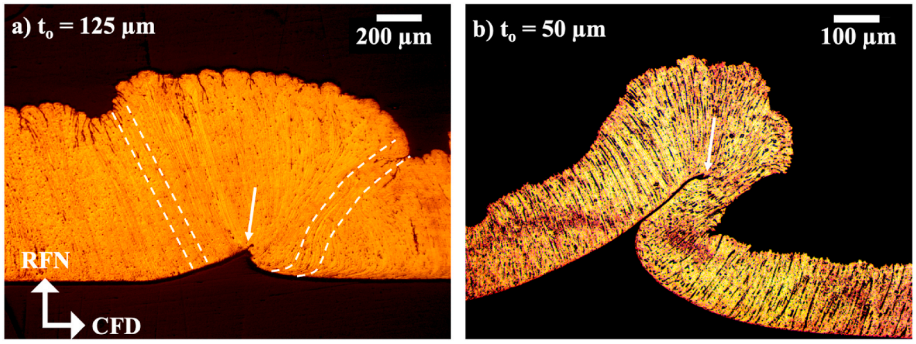

Fig. 8. Micrographs showing a) flow line pattern in a large fold, and b) lift-off of the chip from the rake-face contact due to the severity of the plastic buckling at smaller t_o. The arrows in both figures point to the shear dimple. Note also the crease at arrow in b) formed by compression of the buckle in the dimpled region. AA 8040, $\alpha = 20°$, and $V_o = 3$ m/s.

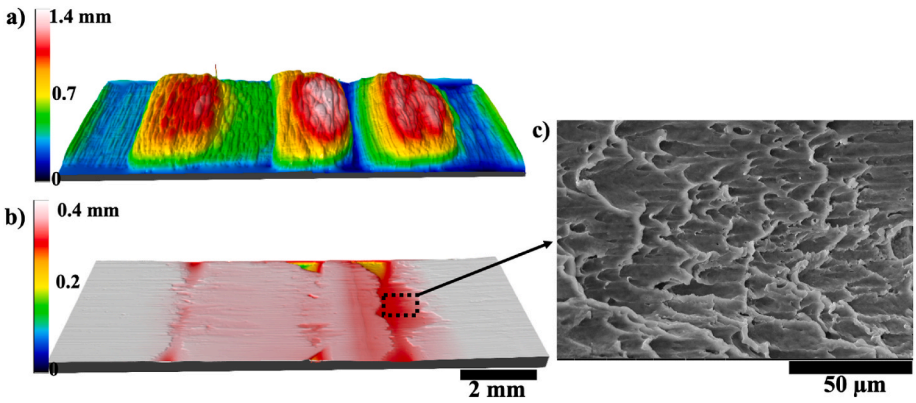

Fig. 9. Surface profiles of a) chip free surface showing the dual-scale folds and b) corresponding chip underside region highlighting the shear dimples and ductile fracture therein. The shear fracture characteristics (e.g., elongated dimple features) within the dimple are highlighted in the enlarged optical micrograph of this region in c). AA 8040, $\alpha = 5^{\circ}$, $t_o = 125$ µm, and $V_o = 3$ m/s. Does the folding persist in successive cutting passes?.

elongated dimples in the depression.

Sometimes, in cutting, a thin deformed surface layer created by a cutting pass can influence the chip formation in subsequent passes, especially with initially annealed metals. As a result, the chip morphology can vary in successive cutting passes. This variation is best illustrated by the large-scale chip thickness oscillations observed when cutting annealed Cu (see Fig. 10). As revealed by high-speed imaging of the cutting zone, the chip thickness varies between two extremum values (thick/thin) across successive cutting passes. When cutting the initially annealed Cu, the chip formed in the first pass is thick, due to sinuous flow and folding (Fig. 10a); but transitions to a significantly thinner chip, with uniform laminar flow, in the second revolution (Fig. 10b and c). This is because in the second pass, the tool is cutting through a highly strained surface layer that has been left behind on the annealed Cu surface after the first pass. In the third revolution/pass, the chip formed is once again thick, like in the first pass (Fig. 10d). This is because, the residual surface layer left behind at the end of the second pass, after cutting through a highly strained surface layer, is no longer that severely strained [22]. Hence, in the third pass, the cutting once again occurs in a largely annealed material (surface layer), with a thick

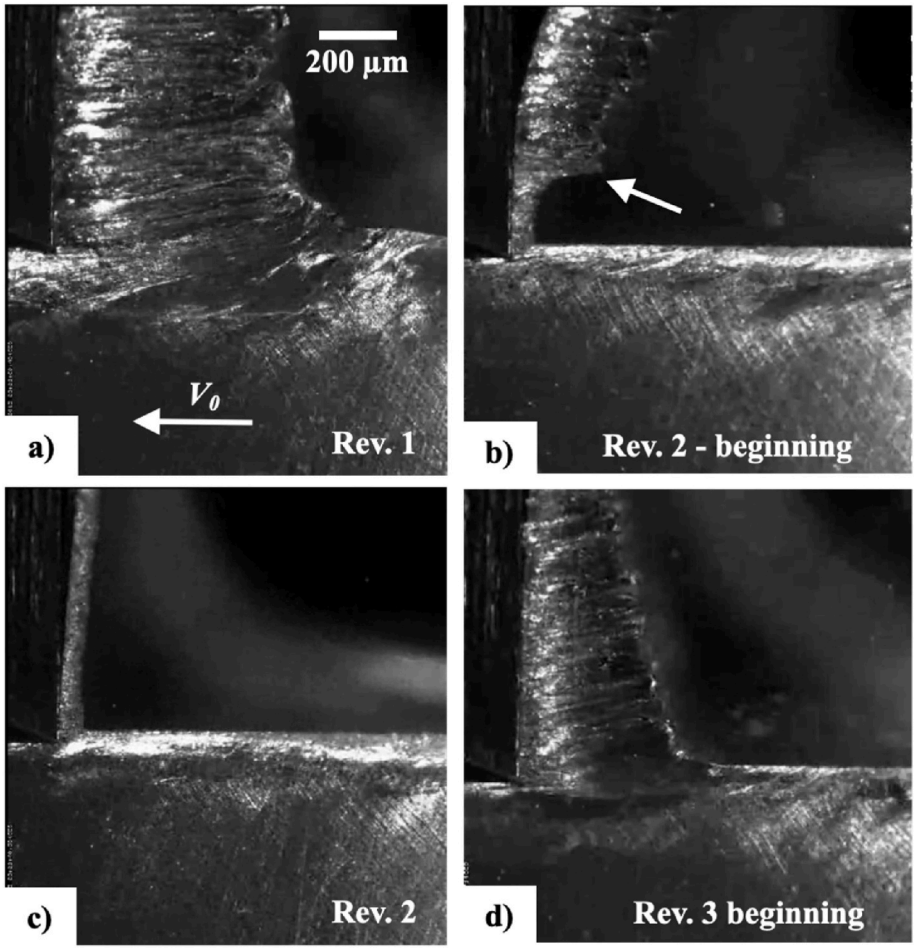

Fig. 10. Chip thickness oscillations in cutting of Cu in an initially annealed condition. a) Thick chip in first pass of cutting over annealed material; b) transition from thick to thin chip at the beginning of the 2nd pass; c) thin chip during the middle of the 2nd pass; and d) transition from thin to thick chip in the beginning stage of the 3rd pass. The oscillations occur due to the effects of the residual plastically strained layers created in the prior cutting pass. $V_o = 100$ mm/s. The tool location is to the left in each frame. Evolution and mechanism of the dual-scale folding.

chip by sinuous flow resulting. This type of recurring chip thickness oscillation persisted throughout the cutting process (100 + passes for the observation duration) in the cutting of the annealed Cu, driven by the changes in the intensity of the deformation of the surface layers produced in successive passes..

This was not, however, the case when cutting the annealed Al alloys. The dual-scale folding was seen to occur over the entire length (>100 revolutions) of the cut in the rotary cutting, with a minimum of at least 8 large-scale folds (with superimposed small folds) forming in each revolution (cutting pass) of the workpiece, see also Supplementary Material Fig. S2. The overall dual-scale folded morphology of the chip remained qualitatively similar over a cutting length of >1 m, indicating that this is the steady-state chip morphology; this may also be inferred from the profilometric traces of the chip back surface in Fig. 9 and the force oscillations in Fig. 12. Thus, any deformed layer created on the workpiece surface by a prior cut did not significantly affect the chip formation in the ensuing pass with the Al.

This observed difference in the cutting behavior of Al and Cu, pertaining to chip morphology and flow patterns in successive passes, likely arises from differences in their strain-hardening behavior and selection of t_o (vis-à-vis surface strained layer thickness). Copper has a much higher strain-hardening exponent (n ~ 0.3) compared to Al (n ~ 0.15), and a much lower stacking fault energy (SFE~90 mJ/m^2 for Cu vs ~250 mJ/m^2 for Al) [23]. A consequence of this SFE difference is that partial dislocations in Cu have a wider equilibrium separation that can impede cross-slip. This difficulty of cross-slip in Cu, coupled with its greater propensity to strain-harden (n ~ 0.3), can result in a much more intense and concentrated surface strain layer on the cut surface of initially annealed Cu (i.e., after the 1st pass). Hence, when cutting through this hardened layer in the second pass, uniform laminar flow and a thin chip can be expected to be the norm (Fig. 10c). With the higher stacking fault energy Al, narrowly-spaced partial dislocations are more likely to result, that can facilitate cross-slip. This, coupled with the smaller strain hardening capacity of Al (n ~ 0.15), should result in a more diffusely strained layer on the cut surface of the annealed Al (Differences of this nature have indeed been noted in recent experiments [6]). Hence, each successive cutting pass in the Al will occur in more of an "annealed" material, with sinuous flow, folding and the dual-scale folded chip morphology resulting at the steady state. Of course, this steady state condition in Al may be expected to change over certain ranges of the undeformed chip thickness [24], depending on the ratio of *to* strained layer thickness.

Based on the flow line pattern and chip lift-off of Fig. 8, the structure of the chip underside as seen in Fig. 9, the comparison with the flow pattern in the small folds (Figs. 6 and 7), and the elimination of the residual strain effects of previous cuts in Al, we can reconstruct a plausible description of how the large folds form. The similarity in the flow line inclinations/rotations, see dashed lines, within the small folds (Fig. 7b) and the large folds (Fig. 8), points to a plastic buckling mechanism (flow instability) also as the cause for the large-fold formation. The nature of the flow line rotation and chip lift-off observed at small undeformed chip thickness in the vicinity of the dimple, suggests that a pinning point develops because of local severe adhesion between chip and tool in the region behind the dimple, and towards the periphery of the tool-chip (intimate) contact length. This adhesive pinning impedes chip motion along the rake face. Consequently, a back pressure (compression) on the chip material can be expected to develop around the dimple region, especially since fresh chip material is continuously emerging, being fed in, from the tool edge. This back pressure causes the chip to plastically buckle in the dimple region, akin to a beam under a compressive load between pinned ends. At small undeformed chip thickness, the buckling can even cause a section of the chip to lift-off from the tool rake face, as seen in Fig. 8b. In the course of the buckling, there is ductile fracture in the dimple region. At small t_o, the two sides of the chip in this region can even form a self-contact or crease because of continued compressive loading. After the buckling and formation of a large fold, the pinning is removed. The cycle then repeats with the formation of a new pinning point, buckling, and folding, and so on. Since the formation of the pinning points occur in an irregular (random) manner, both in space and time, this irregularity explains the largely stochastic nature of the large folds in terms of their spacing (see also Supplementary Fig. S2). This type of plastic buckle (fold) formation, with out-of-plane deformation, will necessarily cause the flow lines to rotate while being centered at the dimple. In contrast to elastic buckling, the plastic buckling is not of the snap-through type. Instead, the buckle develops by gradual out-of-plane deformation with increasing compression back-pressure [25–27].

As to the location of the dimple pinning point - it is well-known that the tool-chip contact along the rake face is characterized by a region of intimate contact, wherein the real and apparent contact areas are equal [15,28,29], followed by a region of less-intimate (intermittent) contact that resembles a conventional sliding contact. The intimate contact

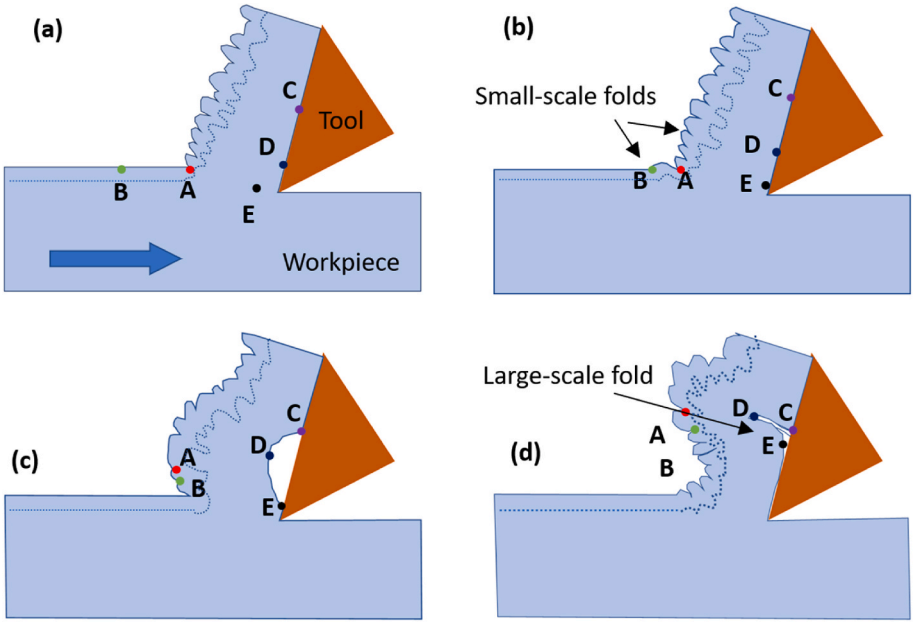

Fig. 11. Schematic of proposed buckling mechanism for the dual-scale fold formation in aluminum cutting. The mechanism can be understood by considering the movement of the five marked points A, B, C, D and E. Points A and B are on the surface of the workpiece, while C, D and E are either in contact with, or eventually reach, the rake face of the chip. (a) The chip at this stage consists of several mushroom shaped features on the surface, which are manifestations of small folds formed earlier. (b) A bump nucleates between (pinning) points A and B by plastic buckling, which is a precursor to the next small fold. At this time, points C, D and E are in contact with the rake face. (c) The bump between the points A and B has now transitioned into a small fold by deformation and rotation of the buckled region. Whenever point C sticks to the rake face, the region between points C, D and E undergoes plastic buckling, losing contact with the rake face - the initial stage in formation of a large fold. (d) With further advance of the tool, the chip continues to form several small folds. Simultaneously, the amplitude of the large fold in region CDE increases, with a crease CDE (self-contact) eventually developing due to local compression for small t_o. This cycle repeats, resulting in small-scale and large-scale folds.

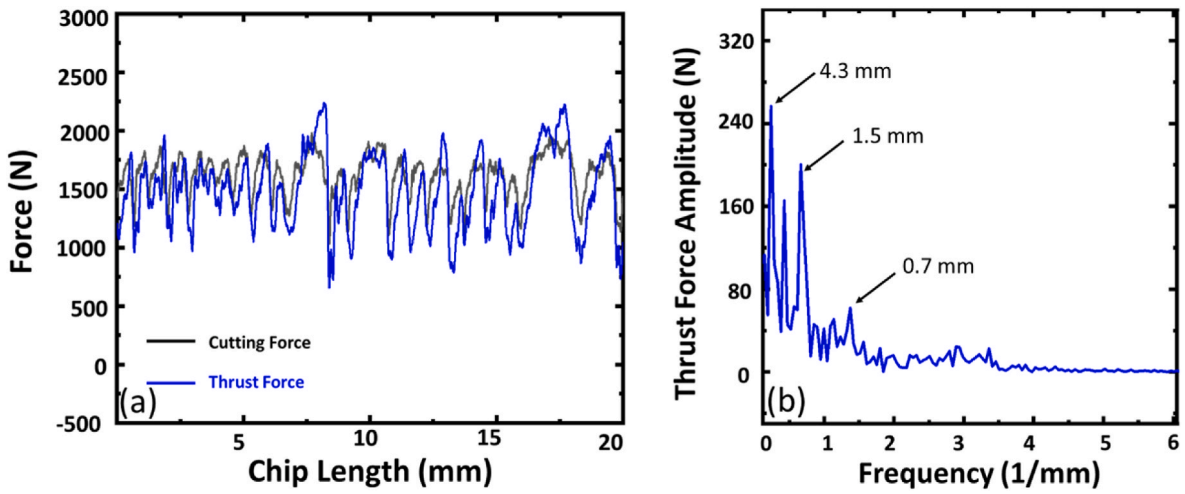

Fig. 12. Force attributes a) Variation of thrust and cutting forces with length of cutting over a region wherein large folds occur. The trace shows force oscillation due to large-fold formation. b) FFT of extended thrust force profile highlighting spatial frequencies corresponding to the large folds in this cutting length. AA 8040, $\alpha = 5^{\circ}$, $t_o = 125$ μm, and $V_o = 6$ m/s.

region typically extends from the cutting edge to some distance along the rake face (approx. 75% of tool-chip contact length), and is characterized by very high normal and shear stresses. Microscopy observations suggest that the pinning point occurs close to the edge of the tool-chip contact length, perhaps in the transition zone between the intimate contact and intermittent contact regions. The trigger (reason) for the recurring formation of pinning points by local adhesion after each buckling event is as yet unknown.

To summarize, the observations suggest the following stages in the development of the chip with the dual-scale fold morphology (see Fig. 11). Fig. 11a shows a snapshot of the workpiece/chip at some point in time. The workpiece is being deformed by the tool at this time to produce a chip with mushroom-like features (prior small folds) on its free surface. The mushroom features are a consequence of repeated small-scale folding, see Fig. 6 and Refs [8,9,22], that has already occurred on the workpiece surface ahead of the advancing tool. To follow the subsequent dual-scale fold development, consider two points on the workpiece surface (A and B) ahead of the tool, and three points in the workpiece that eventually come into contact with the tool rake-surface (C, D and E). A bump nucleates by plastic buckling in the region between points A and B, which are pinned. This is a pre-cursor (nucleation) event for formation of another small-scale fold (Fig. 11b). At this time, points C, D and E are now all in contact with the rake-surface. Due to strong local adhesion between the Al chip and the tool, a material point such as point C sometimes sticks to the rake face while the material trailing it continues to move. This pinning of the material at point C and the resultant compression in the region CDE, causes the CDE to also plastically buckle, resulting in loss of contact with the rake-surface (Fig. 11c); this is the pre-cursor (nucleation) event to a large-scale fold (Note the adhesive pinning does not occur, as is to be expected, under well-lubricated conditions). Meanwhile, as the tool advances, the bump that has formed between points A and B undergoes continued plastic deformation with rotation, developing into a (fully formed) small-scale fold in the chip. Finally, in Fig. 11d, the large-scale fold is also fully developed, with the region CDE becoming a crease (self-contact) due to compression of the larger buckle therein, the analog of Fig. 8b. Also note that at larger t_o, the buckling may occur without gross lift-off (analogous to Fig. 8a) due to an increase in stiffness of the chip (beam) structure. This cycle repeats, with the rake face buckling occurring irregularly, leading to the unique dual-scale fold structures in the chip.

With the large folds occurring quite regularly in certain lengths of the chip, although their overall spatial distribution has a large stochastic element, one can envisage that, the repeated formation and "destruction" of the pinning points in the rake-face contact region, will lead the chip motion to resemble classical stick-slip (jerky motion), such as that seen in the motion of a friction slider in metals [30,31]. In the latter case, the stick-slip arises from repeated material pile-up ahead of the slider (our pinning) followed by fracture in the pile-up region (our buckling); this type of stick-slip is usually accompanied by large force oscillations. Such large force oscillations are also seen in our case, see Fig. 12a, which shows the measured cutting and thrust force (the latter is approximately equal to the force component parallel to the tool rake face, since rake angle is 5°) – and their variation with cutting length in the chip flow direction (CFD). The force oscillations in the figure have peak-to-peak amplitudes in excess of 500 N. An FFT analysis of the thrust force (Fig. 12b) highlights the main frequency components and their (half peak-to-peak) amplitudes. The three principal force frequencies in the figure translate to equivalent fold spacing (wavelength) values of 4.3, 1.5 and 0.7 mm (Fig. 12b). This spacing is in the range of the measured fold spacing from the chip free-surface profiles (Fig. 5) over this length of the chip.

The occurrence of the larger-scale plastic buckling along the rake face of the tool is also supported by a first-order buckling analysis of the chip in this region [9,21,25,26]. Consider a beam (chip) of length 2 mm (large-fold wavelength, roughly equal to length CE in Fig. 11b), width 6 mm (chip width) and thickness 0.7 mm (deformed chip thickness), pinned at both ends, and subjected to an axial force, in our case, the thrust force. If yielding has already occurred in the chip in this rake face region, then plastic buckling of the chip (beam) will occur at a force as small as ~ 270 N. But since the force required to cause yielding in a hardened Al beam of this dimension by uniaxial compression is ~480 N (>270 N), we can conclude that the beam will plastically buckle as soon as this higher yield force of 480 N is reached. Of course, this is only a lower bound on the buckling (thrust) force since the chip (beam) in the present case will be stabilized by the transverse (cutting) force that is imposed approximately normal to the chip-tool contact length. Since the experimentally measured "axial" (thrust) force is ~2000 N (≫ 480 N), see Fig. 12a, we need have no doubts about plastic buckling occurring in the chip. The force observations, both pertaining to the oscillations as well as the buckling analysis, thus provide strong support for the plastic buckling hypothesis and the stick-slip that ensues.

We could rule out other possible sources for the force oscillations such as built-up edge (BUE) formation or system dynamics effects. Optical microscopy did not show any evidence for BUE, and the system-based origin could be eliminated based on stiffness and system-

dynamics characterization.

The specific cutting force, the power component, is also found to be very high ~2000 N/mm^2, with both the Al alloys. And it shows oscillations just like the thrust force (Fig. 12a). Similar force characteristics were observed across the range of cutting speeds to 6 m/s, see Supplementary Material Fig. S1. To calibrate the severity of this cutting force, it is worth recalling that both the Al alloys are very soft, with initial hardness ~25 HV. The specific force value of 2000 N/mm^2 is also much higher (2X to 5X) than what is predicted for equivalent chip shape-transformations, were they to occur purely by homogeneous shear-plane type deformation (laminar flow case) [22]. The very large specific cutting force is thus a consequence of the dual-scale folding and underlying sinuous flow. Consequently, these Al alloys are to be classified as gummy (poor machinability). If the machinability of these alloys is to be improved, it will be necessary to eliminate the sinuous plastic flow mode and replace it with a much less energy-intensive flow mode involving significantly less redundant deformation. Suppression of the plastic buckling and, by extension, the sinuous flow, will also enable the force oscillations to be minimized or eliminated altogether.

4. Folding and plastic buckling: some modeling observations

We use physical modeling structured around finite element analysis and a model (foil) experiment to bring out the critical roles played by pinning of the material flow and plastic buckling in triggering folding at two length scales. The modeling observations provide further support for our folding hypothesis.

4.1. Finite element (FE) modeling of fold development

The small-scale folding phenomenon can be well-captured using a continuum FE model of the cutting that also incorporates grain-level heterogeneity in the material flow stress [32,33]. We discuss this using simulation of cutting of Cu (Fig. 13) for which detailed grain-level flow stress data is available. Prior experimental work has shown that the small-scale folding in annealed Al and Cu is identical. Grain-level flow stress data and assumed grain size distributions for the Cu simulation are the same as in Refs. [32,33].

The FE simulation is seen to well-capture the details of the small-scale folding. Similar to the DIC analysis in Fig. 6, the initial bump development indicated by the yellow arrow (Fig. 13a), follows the origination of pinning points at the thick black line and green line markers with a separation distance >150 μm. The bump begins to slip under an already fully formed fold just ahead of it, initiating a crease or a small self-contact, whose base is marked by the red '+' symbol. In frames b, c, and d, the bump continues to slide under the neighboring fully formed fold, elongating the self-contact (fold) and pushing the base further into the chip. Note that the Lagrangian yellow line in frame a is stretched and rotated in subsequent frames. After self-contact, there is also a characteristic secondary (but perceptible) *local* rotation about the contact point, causing the yellow line to develop an increasingly sharp 'crook' near its free-surface end in frames b, c and d. The solid black line, which is on the other side of the self-contact, is seen to develop a 'crook' in the opposite direction. Also note that the elongation of the Lagrangian yellow line manifests an increment in fold amplitude with a corresponding decrease in the pinning point separation distance to <80 μm (tracking the distance between the green and black line markers in frame a through to d). This mimics a plastically buckled beam loaded under compression at its ends. In frame d, the fold is fully formed while a new, follow-on bump begins to form behind the recently formed fold.

Prior *in situ* studies of cutting annealed Cu, thermally etched to expose the workpiece grain structure, have shown a direct correlation between the grain size and the pinning point separation distance. The initial bump formation – the fold nucleation step – is by plastic buckling of the grains (flow instability) that are pinned at the grain boundaries just ahead of the PDZ [9]. The small-scale folding thus occurs by repeated bump formation between pinning points (likely grain boundaries or analogous defect structures), and subsequent stretching and

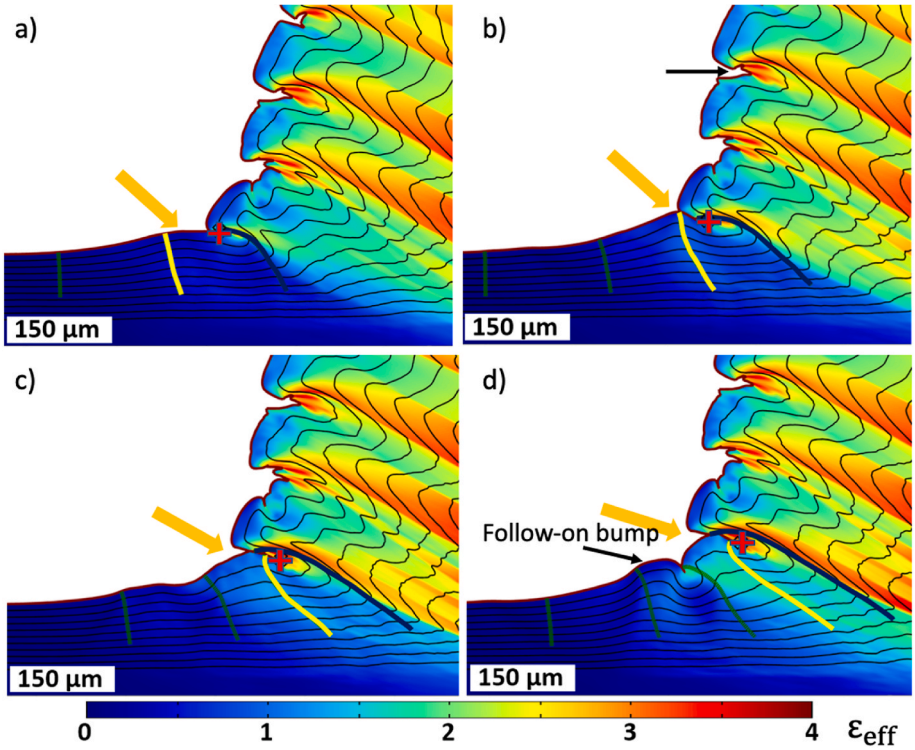

Fig. 13. Finite element simulation showing the development of the small fold formation in annealed Cu. The frames are taken at simulation times t = a) 0.61 s, b) 0.64 s, c) 0.67 s, and d) 0.70 s. The background color shows effective plastic strain. (For interpretation of the references to color in this figure legend, the reader is referred to the Web version of this article.)

rotation of the bumps to form self-contacts (folds). Similar plastic buckling, folding and sinuous flow has been observed in cutting of ductile polymers wherein the buckle size agreed well with that predicted from the forces [21].

While analogous FE simulations of the large-scale fold development along the rake face are difficult, the present simulation findings about the small-scale folds can be extrapolated in the sense that given a pinning mechanism and a sufficiently long 'pinned beam length', fold-formation via buckling is inevitable. Along the rake face, the pinning, which causes the fold nucleation, is promoted by stagnation or reduced flow velocity in the 'stick' phase of stick-slip; this pinning triggers subsequent fold formation. Higher friction along the rake face, while not the primary cause of the large-scale fold nucleation, can however enhance the fold development significantly.

4.2. Plastic buckling at the surface: a model Al foil experiment

Additional illustration of plastic buckling of a thin workpiece surface layer, under conditions analogous to cutting, is provided by the following model experiment. A piece of aluminum foil of thickness ~15 μm was bonded to the surface of OFHC Cu using an adhesive (Gorilla Super Glue). A chip was produced from this material using a zero-degree rake angle tool, $V_o = 0.1$ mm/s, and undeformed chip thickness $t_o = 115$ μm; the t_o value was set so that it was approximately equal to the foil + glue layer thickness. Fig. 14 shows three frames from a high-speed image sequence of the chip formation, with streaklines superimposed onto the Al foil to illustrate the deformation. The foil upon getting fixed between two pinning points P_1 and P_2 (frame a), is seen to undergo out-of-plane deformation gradually with a bump developing between pinning points in the compressive zone ahead of the tool (frame b) – plastic buckling. With further advance of the tool, a full buckle on the surface results with delamination of the foil also occurring. This buckle is rotated and sheared, as it traverses the deformation zone, forming a fold (frame c). The resemblance between the sinuous flow and small-scale folding shown in Figs. 6 and 7, and the buckling-induced flow pattern of Fig. 14 is striking, except for the scale. A similar observation may be made with respect to the formation of the large folds, except that the pinning and compressive buckling here occur in the fully developed chip along the tool rake face.

Interestingly, surface plastic buckling of a similar type has been observed in shear- and tube-spinning processes [34,35], both with deformation zone geometry similar to that in cutting. In these metal deformation processes; the buckling can even lead to delamination of the component being spun from the mandrel on which it is mounted; this is very much akin to our observed chip lift-off and foil delamination.

5. Implications

The observations have shown that with soft, highly strain-hardening alloys like those of aluminum, plastic buckling likely plays a key role in the development of the chip morphology. This chip morphology is characterized by material folding at two different length scales that are roughly one order of magnitude apart (~0.1 vs 2 mm). The small-scale folds are formed by plastic buckling on the workpiece surface, and folding in the deformation zone, just ahead of the advancing tool. The large folds are formed by similar buckling and folding, that is tied to recurring pinning of the chip sliding-motion along the tool rake face. The buckling and folding result in a highly unsteady flow mode, sinuous flow, with large cutting forces, despite the alloys being extremely soft (~25 HV). Furthermore, the large-scale folding, which is triggered by the occurrence of adhesive pinning points at irregular intervals along the tool-chip contact length and which impede chip motion, is concomitant with stick-slip motion of the chip. As a result, oscillations of a large amplitude develop in both the thrust and cutting forces. Similar dual-scale folding and large forces have been observed in cutting of tantalum and niobium alloys, indicating that the same underlying flow phenomena are also operative in these material systems. Effective lubrication of the tool-chip interface region is seen to suppress the large folds, but not the small folds. Lubrication of this interface, however, can be difficult to accomplish in practice at commercial cutting speeds without use of methods such as high-pressure fluid application. The observations confirm once again that the flow mechanism underlying chip formation is reflected in the various length-scale features in the chip morphology, reinforcing the one-to-one correlation between flow and chip morphology that has been consistently observed in the cutting of metals.

The folding has important consequences for machining quality. It results in poor surface finish on the machined surface, with material pull-out and tears [6]. There is evidence also indicating that the residual strain distribution on the machined surface is influenced by the dual-scale folding, though not adversely. In potential applications involving use of machining to produce metal strip and wire by peeling or cutting-extrusion, i.e., materials manufacturing, the dual-scale folding and the high forces are a major barrier to achieving the desired product form. Consequently, there is need to eliminate the "gumminess" in cutting arising from this plastic deformation mode.

Several means for suppressing or minimizing the dual-scale folding are suggested by current and prior work. The first approach is by changing the deformation geometry, mainly by making the rake angle more positive. Fig. 15 is a process map for the Al alloys that demarcates the flow types in cutting speed-rake angle parameter space; this map was constructed from chip observations made at 15 different parameter conditions. The map shows where the different folding mechanisms are operative and when uniform laminar flow prevails. When the rake angle

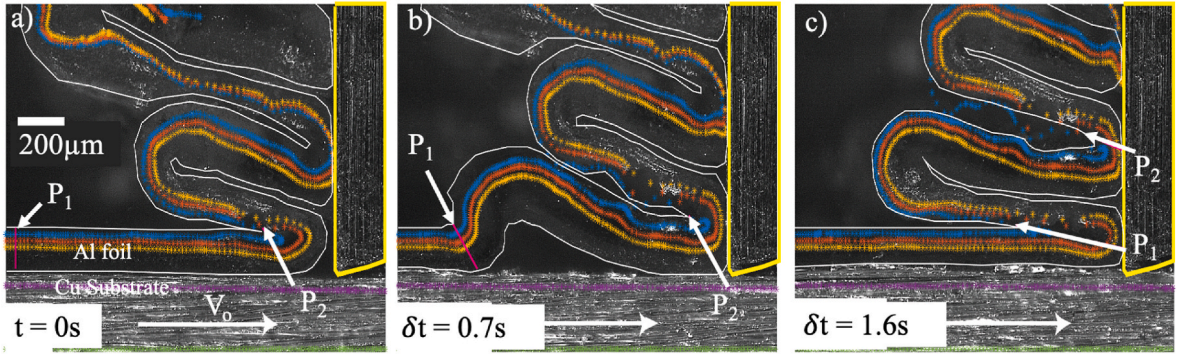

Fig. 14. Select image frames from a model cutting experiment with aluminum foil glued to Cu substrate showing buckling ahead of the primary deformation zone. The buckling is initiated between two pinning points P_1 and P_2 on the workpiece surface in a). In b), a lift-off (buckle) of the foil occurs between the pinning points which subsequently develops into a full fold in c). $V_o = 0.1$ mm/s, $\alpha = 0°$.

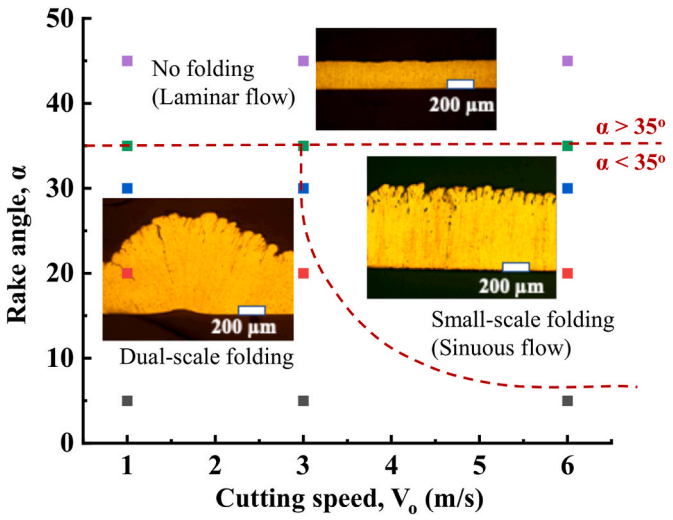

Fig. 15. Process map showing the dominant flow mechanisms with the Al alloys in speed-rake angle parameter space. The insets are chip micrographs produced at the select data point locations. AA 8040, t_o = 125 µm. Dry (unlubricated) cutting condition.

is increased from α = 5° to α = 45°, both the small and large folds decrease in extent across the entire range of cutting speed investigated. Note that purely sinuous flow, without stick-slip along the tool rake face, gives rise only to the small-scale folds. For α > 35°, the folding is generally eliminated with laminar flow becoming the dominant flow mode. But the use of such large positive rake angles may be difficult in practice because of tool wear or fracture issues. Suitable surface texturing of the tool rake face has also been found to enhance the propensity for laminar flow [36].

A second means is via constrained cutting or hybrid cutting-extrusion wherein the exit chip geometry is fixed *a priori* by use of a second constraining tool located directly across from the primary cutting tool in the PDZ. The constrained cutting – hybrid cutting-extrusion – has been shown to suppress and even fully eliminate many plastic flow instabilities such as shear banding, segmentation and buckling [4]. This suppression mechanism needs to be explored, however, in the context of the large folds. A third approach involves mechanochemical means, using organic surface-adsorbing films that can trigger a local ductile-to-brittle transition in material behavior on the workpiece surface in the primary deformation zone (PDZ) [14,37]. The embrittlement also causes the forces to be significantly lowered, and the machined surface quality to be improved both in terms of surface finish (smoother surface) and residual plastic strain (reduction). While this approach has been shown to eliminate the smaller-scale folds that form in the PDZ [37], as to how this mechanochemical route will change (or suppress) the larger-scale folding is as yet unknown. Based on both force and surface quality considerations, the mechanochemical approach is likely the best route for realizing major improvements in machining performance with the gummy metals, provided some implementation issues can be solved. The various potential routes for suppressing or minimizing the dual-scale folding are currently under investigation.

6. Conclusion

A chip morphology, characterized by dual-scale folding and occurring in cutting of relatively soft, highly strain-hardening metals, has been studied with very soft aluminum alloys (hardness ~ 25 HV), using *ex situ* characterization of chip attributes and *in situ* analysis of material flow. It is shown that the small-scale folds form by folding of material in the primary deformation zone (PDZ), triggered by plastic buckling instability in a thin surface layer of material on the workpiece surface ahead of the PDZ and advancing tool. The large-scale folds form as the chip traverses the rake face, again as a result of plastic buckling due to the chip motion being impeded by recurring adhesive pinning of the chip, albeit at irregular intervals, along the rake face. Their occurrence is largely stochastic due to the irregular nature of the pinning. The large fold formation is concomitant with stick-slip motion of the chip along the rake face. The sinuous flow mode, which arises from the small-scale folding, and the stick-slip, associated with the large folds, both cause the cutting forces to be very large and to also oscillate with large amplitude. These large forces and oscillations arise despite the metal systems being very soft. The dual-scale folding chip morphology is shown to have a one-to-one correlation with the underlying flow mode and plastic instability phenomena in the cutting zone, consistent with what has been observed in the past with other unsteady and steady flow modes. Several methods have been identified and briefly discussed for reducing or potentially eliminating the undesirable dual-scale folding.

Credit author statement

Mohammed Naziru Issahaq: Conceptualization, Methodology, Investigation, Writing - Original Draft, Formal Analysis; Anirudh Udupa: Validation, Formal Analysis, Software, Writing – Review & Editing; Mojib Saei: Investigation, Validation, Software; Debapriya Pinaki Mohanty: Investigation, Validation, Formal Analysis; James B. Mann: Resources, Supervision, Writing – Review & Editing; Narayan K. Sundaram: Investigation, Software, Validation; Kevin P. Trumble: Resources, Supervision, Writing – Review & Editing, Project Administration, Funding Acquisition; Srinivasan Chandrasekar: Resources, Supervision, Writing – Review & Editing, Project Administration, Funding Acquisition.

Declaration of competing interest

The authors declare that they have no known competing financial interests or personal relationships that could have appeared to influence the work reported in this paper.

Data availability

Data will be made available on request.

References

[1] M.E. Merchant, Mechanics of the metal cutting process. I. Orthogonal cutting and a type 2 chip, J. Appl. Phys. 16 (1945) 267–275, https://doi.org/10.1063/1.1707586.
[2] M.C. Shaw, Metal Cutting Principles, second ed., Oxford University Press Inc, New York, 2005.
[3] K. Nakayama, the formation of "saw-toothed chip" in metal cutting, Proceedings of the International Conference on Production Engineering (1974) 572–576, https://doi.org/10.2493/jjspe1933.43.117.
[4] D. Sagapuram, A. Udupa, K. Viswanathan, J.B. Mann, R. M'Saoubi, T. Sugihara, S. Chandrasekar, On the cutting of metals: a mechanics viewpoint, J. Manuf. Sci. Eng. 142 (2020), https://doi.org/10.1115/1.4047869.
[5] Z. Liao, A. la Monaca, J. Murray, A. Speidel, D. Ushmaev, A. Clare, D. Axinte, R. M'Saoubi, Surface integrity in metal machining - Part I: fundamentals of surface characteristics and formation mechanisms, Int. J. Mach. Tool Manufact. 162 (2021), 103687, https://doi.org/10.1016/j.ijmachtools.2020.103687.
[6] M.N. Issahaq, A. Udupa, T. Sugihara, D.P. Mohanty, J.B. Mann, K.P. Trumble, S. Chandrasekar, R. M'Saoubi, Enhancing surface quality in cutting of gummy metals using nanoscale organic films, CIRP Annals 71 (2022) 93–96, https://doi.org/10.1016/j.cirp.2022.04.078.
[7] R. Komanduri, B.F. Von Turkovich, New observations on the mechanism of chip formation when machining titanium alloys, Wear 69 (1981) 179–188, https://doi.org/10.1016/0043-1648(81)90242-8.
[8] H. Yeung, K. Viswanathan, W.D. Compton, S. Chandrasekar, Sinuous flow in metals, Proc. Natl. Acad. Sci. USA 112 (2015) 9828–9832, https://doi.org/10.1073/pnas.1509165112.
[9] A. Udupa, K. Viswanathan, Y. Ho, S. Chandrasekar, The cutting of metals via plastic buckling, Proceedings of the Royal Society A 473 (2017), 20160863, https://doi.org/10.1098/rspa.2016.0863.
[10] ASM Handbook, Machining of Aluminum and Aluminum Alloys, ASM International, 1989, https://doi.org/10.31399/asm.hb.v16.a0002184.

[11] M.N. Issahaq, S. Chandrasekar, K.P. Trumble, Single-step shear-based deformation processing of electrical conductor wires, J. Manuf. Sci. Eng. 143 (2021) 1–9, https://doi.org/10.1115/1.4048984.
[12] T. Kaneeda, M. Yamada, L. Anthony, chip formation mechanism of pure niobium plates in a superconducting accelerator cavities, in: Proc. 13th Int. Conf. Eur. Soc. Precis. Eng. Nanotechnol. EUSPEN 2013 vol. 2, 2013, pp. 129–132.
[13] K. Sakai, K. Shintani, H. Kato, Study on the cutting mechanism of tantalum materials, Proceedings of JSPE Spring Conference (2011) 239–240.
[14] J.M. Davis, M. Saei, D.P. Mohanty, A. Udupa, T. Sugihara, S. Chandrasekar, Cutting of tantalum: why it is so difficult and what can Be done about it, Int. J. Mach. Tool Manufact. 157 (2020), 103607, https://doi.org/10.1016/j.ijmachtools.2020.103607.
[15] E.M. Trent, Metal Cutting, Butterworth, London, 1977.
[16] D.G. Altenpohl, Aluminum: Technology, Applications, and Environment: A Profile of a Modern Metal, sixth ed., Aluminum Association, Washington, DC, 1998.
[17] ASM Handbook, Properties and Selection: Nonferrous Alloys and Special-Purpose Materials, ASM International, USA, 1990.
[18] J.E. Hatch, Microstructure of alloys, in: Aluminum Properties and Physical Metallurgy, 1984, pp. 58–104, https://doi.org/10.13618/appm1984p058.
[19] H. Okamoto, M.E. Schlesinger, E.M. Mueller, Aluminum binary alloy phase diagrams, in: Alloy Phase Diagrams, ASM International, 2016, pp. 113–139, https://doi.org/10.31399/asm.hb.v03.a0006144.
[20] R.J. Adrian, J. Westerweel, Particle Image Velocimetry, Cambridge University Press, 2011.
[21] A. Udupa, K. Viswanathan, S. Chandrasekar, Pattern formation on free surfaces via plastic buckling and periodic folding, Europhys. Lett. 129 (2020), 46001, https://doi.org/10.1209/0295-5075/129/46001.
[22] H. Yeung, K. Viswanathan, A. Udupa, A. Mahato, S. Chandrasekar, Sinuous flow in cutting of metals, Phys. Rev. Applied. 8 (2017), 054044, https://doi.org/10.1103/PhysRevApplied.8.054044.
[23] R.W. Hertzberg, R.P. Vinci, J.L. Hertzberg, Deformation and Fracture Mechanics of Engineering Materials, fifth ed., Elsevier, NJ, US, 2013 https://doi.org/10.1016/B978-0-08-026167-6.50013-8.
[24] S. Zaima, K. Takimizu, Some considerations on the mechanics of aluminium machining, Bulletin of JSME 13 (1970) 719–723, https://doi.org/10.1299/jsme1958.13.719.
[25] S.H. Crandall, N.C. Dahl, T.J. Lardner, An Introduction into the Mechanics of Solids, McGraw-Hill, New Delhi, 1978.
[26] F.R. Shanley, Inelastic column theory, J. Aeronaut. Sci. 14 (1947) 261–268, https://doi.org/10.2514/8.1346.
[27] Z.P. Bazant, L. Cedolin, Stability of Structures: Elastic, Inelastic, Fracture and Damage Theories, World Scientific, Singapore, 2010.
[28] E.D. Doyle, J.G. Horne, D. Tabor, Frictional interactions between chip and rake face in continuous chip formation, Proceedings of the Royal Society of London. A. Mathematical and Physical Sciences 366 (1979) 173–183, https://doi.org/10.1098/rspa.1979.0046.
[29] N.N. Zorev, Metal Cutting Mechanics, Pergamon Press, 1996.
[30] E. Rabinowicz, Stick and Slip, Scientific American Inc., 1956, pp. 109–119.
[31] F.P. Bowden, D. Tabor, Friction; an Introduction to Tribology, Anchor Press, New York, 1973.
[32] A.S. Vandana, N.K. Sundaram, Simulation of sinuous flow in metal cutting, Tribol. Lett. 66 (2018) 94, https://doi.org/10.1007/s11249-018-1047-5.
[33] A.S. Vandana, N.K. Sundaram, Simulation of machining of ductile polycrystalline aggregates using a remeshing framework, J. Manuf. Process. 54 (2020) 1–13, https://doi.org/10.1016/j.jmapro.2020.02.041.
[34] S. Kobayashi, Instability in conventional spinning of cones, Journal of Engineering for Industry 85 (1963) 44–48, https://doi.org/10.1115/1.3667585.
[35] S. Kalpakjian, S. Rajagopal, Spinning of tubes: a Review, J. Appl. Metalwork. 2 (1982) 211–223, https://doi.org/10.1007/BF02834039.
[36] T. Sugihara, R. Kobayashi, T. Enomoto, Direct observations of tribological behavior in cutting with textured cutting tools, Int. J. Mach. Tool Manufact. 168 (2021), https://doi.org/10.1016/j.ijmachtools.2021.103726, 103726.
[37] T. Sugihara, A. Udupa, K. Viswanathan, J.M. Davis, S. Chandrasekar, Organic Monolayers Disrupt Plastic Flow in Metals, Sci. Adv.. 6 (n.d.) eabc8900. https://doi.org/10.1126/sciadv.abc8900.